HHS Public Access

Author manuscript

*Nanoscale*. Author manuscript; available in PMC 2016 May 07.

Published in final edited form as:

*Nanoscale*. 2015 May 7; 7(17): 7780–7789. doi:10.1039/c3nr04421a.

# Functionalized Iron Oxide Nanoparticles for Controlling the Movement of Immune Cells

**Ethan E White**[a,c,e], **Alex Pai**[d,e], **Yiming Weng**[a,e], **Anil K. Suresh**[a,e], **Desiree Van Haute**[a,c], **Torkom Pailevanian**[d], **Darya Alizadeh**[a,b], **Ali Hajimiri**[d,*], **Behnam Badie**[b,*], and **Jacob M. Berlin**[a,*]

[a]Department of Molecular Medicine, 1500 East Duarte Road, Duarte, CA, 91010, United States

[b]Division of Neurosurgery, Department of Surgery, Beckman Research Institute, 1500 East Duarte Road, Duarte, CA, 91010, United States

[c]Irell & Manella Graduate School of Biological Sciences at City of Hope, 1500 East Duarte Road, Duarte, CA, 91010, United States

[d]Department of Electrical Engineering, California Institute of Technology, 1200 E. California Blvd., Pasadena, CA 91125, United States

## Abstract

Immunotherapy is currently being investigated for the treatment of many diseases, including cancer. The ability to control the location of immune cells during or following activation would represent a powerful new technique for this field. Targeted magnetic delivery is emerging as a technique for controlling cell movement and localization. Here we show that this technique can be extended to microglia, the primary phagocytic immune cells in the central nervous system. The magnetized microglia were generated by loading the cells with iron oxide nanoparticles functionalized with CpG oligonucleotides, serving as a proof of principle that nanoparticles can be used to both deliver an immunostimulatory cargo to cells and to control the movement of the cells. The nanoparticle-oligonucleotide conjugates are efficiently internalized, non-toxic, and immunostimulatory. We demonstrate that the *in vitro* migration of the adherent, loaded microglia can be controlled by an external magnetic field and that magnetically-induced migration is non-cytotoxic. In order to capture video of this magnetically-induced migration of loaded cells, a novel 3D-printed “cell box” was designed to facilitate our imaging application. Analysis of cell movement velocities clearly demonstrate increased cell velocities toward the magnet. These studies represent the initial step towards our final goal of using nanoparticles to both activate immune cells and to control their trafficking within the diseased brain.

[*]Drs. Hajimiri, Badie, and Berlin, served as co-PI’s for these studies. Contact info: jberlin@coh.org. Tel.: +1 626 256 4673, bbadie@coh.org. Tel.: +1 626 256 4673. hajimiri@caltech.edu. Tel.: +1 626 395 2312.

[e]These authors contribute equally.

**Electronic Supplementary Material:** Supplementary material with the transmission electron microscopy images of the particles, additional independent experiments for the NFκB activity and exocytosis assays, TEM images for the SPION untreated cells, bright field microscopy images of the cells alone in the presence and absence of magnet, images of the magnetic movement experiments at higher doses of SPION, full uncropped images of the post-migration LIVE/DEAD assay, and a video file of cell movement is available in the online version of this article.

## 1. Introduction

Immunotherapy is an attractive treatment strategy for many diseases, including cancer.[1] Generally, this strategy involves stimulating the immune system such that it recognizes the diseased cells as foreign and eliminates them. A wide variety of agents, ranging from antibodies, to engineered immune cells, to potent adjuvants have been used to stimulate the immune system. Immunotherapy would be greatly enhanced as a treatment strategy if the location of the immune cells both during and after stimulation could be controlled. For the case of cancer immunotherapy, it could be of great benefit to direct activated immune cells to the tumor in order to promote antigen recognition specifically for cancer cells. Furthermore, the immune response could be enhanced by maintaining a population of activated immune cells at the primary tumor site and/or improving the trafficking of activated immune cells to distant foci of disease.

We have been pursuing the use of oligodeoxynucleotides that contain an unmethylated CpG motif (CpG) as immune stimulants for the treatment of glioblastoma. CpG is known to be immunostimulatory by activating toll like receptor-9 (TLR9) which is expressed by normal and glioma-associated human microglia and macrophages.[2–5] Activation of TLRs enhances the uptake of microorganisms by phagocytic cells, promotes secretion of Th1 cytokines, and mediates leukocyte recruitment to infected tissues. TLR9 is not found on the cell surface, but is initially located in the endoplasmic reticulum (ER) and is then found colocalized with CpGs in the lysosomes following stimulation.[6] Therefore, because CpG-induced immune stimulation is dependent upon TLR9 interacting with CpG inside the endosomal compartment, using a platform that achieves endosomal delivery of CpG may be an attractive strategy for enhancing CpG efficacy.[7]

Nanoparticles are appealing delivery platforms for CpG because, in general, nanoparticles are rapidly endocytosed by phagocytic immune cells.[8] Various nanoparticles have been investigated as potential candidates for the delivery of CpGs, including liposomes,[9] self-assembling DNA nanoparticles,[10] poly(lactic-co-glycolic acid) nanoparticles[11] and gold nanoparticles.[12] For the treatment of brain cancers, we recently reported that the use of single-walled carbon nanotubes as delivery vehicles for CpG dramatically increased the efficacy of the CpG, such that a *single* intracranial injection of the nanotube-CpG construct cured 60% of glioma-bearing mice.[13, 14] Moreover, when mice that were cured by treatment with the nanotube-CpG construct were rechallenged with a subcutaneous injection of GL261 glioma cells, every mouse rejected the cancer cells, demonstrating a successful induction of systemic immunity.

This nanotube-CpG construct is readily taken up by macrophages, microglia, NK cells and dendritic cells.[13] We hypothesized that using super paramagnetic iron oxide nanoparticles (SPIONs) as the delivery platform for the CpG would enable magnetic control of immune cells that endocytosed the particles. SPIONs respond to magnetic fields and allow for the controlled delivery of conjugated chemotherapeutics.[15] This technique may even allow for targeted delivery deep within the body.[16, 17] Magnetic targeting of drug delivery has been applied to brain tumors.[18] Recently, magnetic targeting has been extended to cells by labeling desired cell populations with SPIONs and other magnetic particles. One focus of

this work has been attracting loaded cells to magnetized implanted devices, such as stents.[19, 20] Another primary application has been targeting loaded stem cells for regenerative medicine.[21–24] A limited number of publications have also described magnetic control of loaded immune cells.[25] Clinically, we envision that a SPION-based immunotherapy could be injected intracranially, internalized by local immune cells, and then enable the magnetically-controlled migration of these activated immune cells for the treatment of multifocal disease or deep brain tumors.

Here we demonstrate that SPION-CpG conjugates are efficiently internalized by microglia which allows for magnetic control of the loaded cells. The synthesis and characterization of the SPION-CpG conjugates is described. Furthermore, the SPION-CpG conjugates are shown to be non-toxic and immunostimulatory.

## 2. Results and discussion

The long-term goal of this research is to generate an iron-oxide-based cancer immunotherapy that enables magnetically-guided, modular localization of activated immune cells *in vivo*. The objective of this manuscript is to provide proof-of-principle evidence that adherent, microglia-like immune cells can be loaded with immunostimulatory particles and moved by magnetic fields *in vitro*. To perform the *in vitro* magnetic field influenced cell movement studies, SPION-CpG conjugates (Fig 1A) were prepared from 30 nm SPIONs (Fig S1A). The synthetic protocol was intended to produce CpG conjugated to PEG with a terminal silyl ether for conjugation to the SPIONs, but Mass Spectrometry (MS) analysis (Fig S1C) indicated that the reduction of RSSCpG was inefficient and thus the majority of material used to coat the SPIONs was likely RSSCpG. Nonetheless, it was clear that a functional coating was achieved as demonstrated by the change in aqueous stability of the SPIONs. The as-received SPIONs were coated with oleic acid and thus not miscible with water, but, following sonication with the CpG-containing material, the SPIONs entered the aqueous phase. Furthermore, zeta potential measurements showed the resulting SPION-CpG particles to be negatively charged, consistent with an oligonucleotide coating (Fig 1B). Dynamic light scattering measurements indicated that the SPION-CpG conjugates have a hydrodynamic diameter of 94±5 nm, as compared to 46±2 nm for the free SPIONs (Fig 1B). This is likely the result of small aggregates forming following the coating, as revealed by transmission electron microscopy (TEM, Fig 1C).

Cell assays indicated that SPION-CpG was both non-cytotoxic (Fig 1D) and immunostimulatory (Fig 1E). The LIVE/DEAD assay was used to evaluate cell viability of N9 mouse microglia cells after 12 h of loading at SPION-CpG concentrations up to 0.5 mg/mL. As shown in Fig 1D and Fig S1D, the treated cells exhibited an equivalent level of viability as untreated control cells. In order to evaluate the immunostimulatory potential of SPION-CpG, an NFκB reporter cell line was used. Because NFκB activity is increased in response to TLR9 activation by CpG, immune stimulation by SPION-CpG was expected to cause an increase in NFκB signal within this reporter system. Indeed, SPION-CpG treatment induced an increase in NFκB activity when compared to untreated cells (Fig 1E). However, the NFκB activity of SPION-CpG was less than an equivalent amount of free CpG (RSSCpG). This reduction in activity has several possible causes. It is possible that some

CpG was lost during the SPION-CpG synthesis process, thus resulting in lower NFκB activity after uptake by reporter cells. It is also possible that the immunostimulatory activity of CpG was partially inhibited by conjugation to SPIONs. Phosphate groups are well-known for their ability to bind the surface of iron oxide.[26, 27] Therefore it is likely that the phosphorothioate backbone of the CpG oligonucleotide interacted with the surface of the SPIONs, interfering with CpG release or its binding to TLR9.[28] Future work will focus on investigating the mechanism of this phenomenon and further enhancing the immunostimulatory activity of SPION-CpG.

Next, inductively coupled plasma mass spectrometry (ICP-MS) was used to quantify the cellular uptake of the SPION-CpG by N9 microglia. Briefly, cells were treated with increasing concentrations (0, 0.01, 0.1, 0.3 and 0.5 mg/mL) of SPION-CpG conjugates for 12 h, washed thoroughly, digested with nitric acid and analyzed using ICP-MS. A dose-dependent increase in iron content above the normal background level in control cells was observed (Fig 2E). For comparison, cells were also treated with the commercially available Ferumoxytol iron oxide nanoparticles (sold under the name Feraheme®), which are approved for human use by the US Food and Drug Administration. Ferumoxytol particles are similar in size to the SPIONs used in this study, with an iron core diameter of 17–30 nm.[29] However, even when cells were exposed to a 3× higher concentration of Ferumoxytol as compared to SPION-CpG, very little uptake of the Ferumoxytol particles was observed. While there are a number of differences between our SPION-CpG and Ferumoxytol, we speculate that this increased loading of SPION-CpG was due to the oligonucleotide coating. It has previously been shown that oligonucleotide coatings lead to enhanced cell uptake mediated by scavenger receptors.[30, 31] Independent of the mechanism responsible, the enhanced uptake for our SPION-CpG made this material appealing for use in the magnetic control of microglia.

Further, dark-field microscopy imaging was performed to show the uptake and distribution of the particles over a relatively large area. N9 cells treated with SPION-CpG conjugates at a concentration of 0.5 mg/mL were assessed using a dark-field microscope. Untreated control cells showed no uptake (Fig 2A), whereas cells treated with SPION-CpG conjugates showed profound uptake of the SPIONs (Fig 2B). TEM imaging was also performed to gather information on the intracellular distribution of the SPION-CpG conjugates. At low magnification, TEM imaging performed across various regions of the grid revealed strong uptake of the SPION-CpG conjugates, in agreement with dark-field microscopy. Higher magnification TEM imaging showed dense aggregates of particles that were predominantly located in intracellular vesicles (Fig 2C–D). Some particles were observed in the cytoplasm as well, and no particles were found in the nucleus. Similarly, no uptake was observed in the untreated control cells (Fig S2A–B).

After verifying that SPION-CpG was internalized by N9 cells, the exocytosis of these particles was then investigated. This has important implications in experiments involving magnetically-induced movement. As a cell exocytoses SPIONs, its responsiveness to magnetic fields will decrease as a function of the amount of residual intracellular iron. Thus the rate of exocytosis affects the time period over which the cells can be moved *in vitro*. In order to track the rate of exocytosis, N9 cells were loaded and the iron content of both the

cells and the cell media was measured at 0, 8, and 24 h after loading. Over a 24 h period, there was no detectable increase in the iron content of the cell media nor was there a detectable decrease in the iron content of the cell fraction (Fig 2F). Therefore, we concluded that exocytosis of SPION-CpG was negligible in N9 cells over 24 h. The background iron level in the media at 0 h was presumably residual free SPION-CpG which was not removed when the loaded cells were washed with PBS two times. Longer time points were not investigated because 24 h proved sufficient to demonstrate robust *in vitro* movement.

As a simple test to evaluate if SPION-CpG-loaded microglia could be controlled with an external magnetic field, three different shaped magnets were placed underneath glass bottom culture dishes containing adherent N9 cells loaded with SPION-CpG. After 20 h, the media was aspirated, the plates were stained with Prussian blue, and photographs were taken to demonstrate the shape-dependent localization of the loaded cells (Fig 3A). Additionally, this magnetically controlled cell movement was correlated with the dose of SPION-CpG given to the cells, with higher loadings leading to more pronounced accumulation at the magnet (Fig S3A–C). As controls, we also imaged SPION-CpG particles only with magnet exposure, untreated cells with magnetic exposure and cells loaded with SPION-CpG that were not exposed to any magnets. The SPION-CpG only control shows almost no adherence of the particles, such that following staining and washing, very little material remained in the dish (Fig 3D). Neither “empty” cells that were exposed to the magnet nor loaded cells not exposed to the magnet migrated *in vitro*, confirming that the shape-dependent localization of the loaded cells was magnetically controlled (Fig 3B–C). In order to more closely monitor the magnetically induced migration of the cells, higher magnification images were recorded for loaded cells after 0, 2, 4, and 20 h of magnet exposure (Fig S4M–P). Accumulation of the loaded cells at the edge of the magnet where the magnetic field gradient was largest was observed by 4 h and increased until 20 h. Collectively, these controls demonstrate that the accumulation at the edge of the magnet was due to SPION-loaded cells moving in response to the magnetic field.

In order to verify that magnetically-induced movement was nontoxic, the migrated cells were examined for changes in viability and cell morphology. Because the migrated cells comprise only a small percentage of the total cell population of the dish, assays that analyze the bulk cell population would not be able to detect changes in the migrated cell population due to a high background signal from the non-migrated cells. Furthermore, there is no good way to separate the migrated and non-migrated cell populations prior to analysis. Therefore, analysis of the migrated population was performed using imaging-based techniques. Imaging-based techniques allow the spatial information from the cells to be preserved during the analysis, enabling quick identification of migrated and non-migrated populations.

Viability and cell morphology were examined via the LIVE/DEAD assay and SEM, respectively. After loaded cells were exposed to the magnet for 20 h and clear migration was observed, the cells in the dish were stained with calcein AM and ethidium homodimer, fixed, and then fluorescently imaged to assess viability. After fluorescent imaging, the same region of cells was imaged by SEM. No decrease in cell viability was detected for migrated cells nor were any gross abnormalities in cell morphology observed (Fig 3E–H, S3D–G).

The movement of magnetized cells is primarily determined by the external magnetic field profile and strength, the hydrodynamic properties of the cell in its environment, and the effectiveness of SPION uptake by the cells. An important evaluation of cell motility is the quantification of movement velocity. Therefore, in order to analyze the movement velocity of cells, an innovative imaging, incubation, and magnetic manipulation apparatus was designed to track magnetized cells in magnetic fields (Fig S4Q). The apparatus consists of a custom “cell box” fitted onto a standard sized petri dish. N9 cells were plated onto the coverslip portion of the cell box and then loaded with SPION-CpG. After cell loading, the entire box assembly was then inverted into a petri dish containing culture medium. For time-lapse imaging, the cell box and petri dish were placed onto the stage of an inverted microscope equipped with incubation capabilities. A ceramic permanent magnet was then placed on the opposite side of the coverslip to which the cells were attached.

During magnet exposure, the cells were imaged at 2 frames/min for a period of 20 h. Cell positions were extracted using an image processing algorithm.[32] The distribution of cell velocities in the vertical direction (toward the magnet) and horizontal direction is shown in Fig 4A–B. The histograms in Fig 4A–B show that the cell movement in the horizontal direction was symmetrical, while cell movement in the vertical direction was skewed toward the externally-applied magnetic field. In some cases cells migrated toward the magnet at velocities exceeding 30 μm/min.

## 3. Experimental

Ultrasonication was performed using a QSONICA Sonicator Q700 (QSONICA, Newtown, CT, USA) equipped with a cup horn cooled with running water from the sink. Super paramagnetic iron oxide nanoparticles (30 nm, catalogue #SOR-30) were purchased from Ocean Nanotech, Springdale, AR, USA. Silane-PEG-$NH_2$ (MW = 2000, Catalogue #PG2-AMSL-2k) was purchased from NANOCS. Dithiotheritol (DTT) was purchased from VWR. Fully phosphorothioated CpG oligonucleotides bearing a terminal dithiol (5-HO-$C_6$-SS-$C_6$-T*A*A*A*C*G*T*T*A*T*A*A*C*G*T*T*A*T*G*A*C*G*T*C*A*T*-3) (RSS-CpG) was provided by the DNA core facility at Beckman Research Institute at City of Hope. Sulfosuccinimidyl 6-(3'-[2–pyridyldithio]-propionamido)hexanoate (Sulfo-LC-SPDP) was purchased from ProteoChem (catalogue #c1118). Illustra NAP-25 columns (catalogue #17-0852-01) were purchased from GE Healthcare. All other chemicals and reagents were from standard commercial sources. N9 cells were cultured in Dulbecco's Modified Eagle Medium (with high glucose, L-glutamine, sodium pyruvate) supplemented with 10% fetal bovine serum (FBS), HEPES (0.01M), penicillin (100 U/mL), and streptomycin (100 μg/mL) incubated at 37°C in a humidified 5% $CO_2$ atmosphere. For movement experiments, cells were cultured in glassbottom dishes (MatTek Corporation, catalogue # P35G-0-14-C). Coverslip removal fluid (catalogue # P DCF OS 30) was obtained from MatTek.

### 3.1. SPION-CpG synthesis

Silane-PEG-$NH_2$ (29 eq, 17mM) and Sulfo-LC-SPDP (17 eq, 10mM) were dissolved in deionized water and stirred for 2 hours at room temperature. Meanwhile, RSS-CpG (1 eq) was dissolved in deionized water containing at least 2.5mM DTT and stirred for 2 hours at

room temperature. DTT-treated RSS-CpG was then passed through a nap-25 column (GE Healthcare) in order to remove excess DTT. The CpG solution was then added to the Silane-PEG-$NH_2$-containing reaction and heated in a 60 °C oil bath for at least 2 hours. After 2 hours, the reaction was isopropanol-precipitated, dialyzed against deionized water using a <3.5kD MWCO membrane, and lyophilized.

The lyophilized material was dissolved in deionized water and diluted to an effective CpG concentration of 2 mg/mL based on UV absorbance at 260 nm (RSSCpG $\varepsilon_{260nm}$ = 261900 L $mol^{-1}$ $cm^{-1}$). Then SPIONs (25 mg/mL in chloroform) were combined with the product stock solution in a 1:1 mass ratio (SPION : CpG). The mixture was rotated for 10 minutes and distributed into 1.5 mL microcentrifuge tubes with <1 mL in each. To disperse the SPIONs, the sample tubes were ultrasonicated for a process time of 4 h (80 amplitude, 15 s on, 15 s off). The SPION-CpG conjugates were then dialyzed (100 kD MWCO) against deionized water. After dialysis, the samples were diluted to a final concentration of 1 mg/mL SPIONs and 1 mg/mL RSSCpG (assuming no loss) using deionized water. During synthesis of SPION-CpG, discoloration of sample tubes and sedimentation upon dialysis membranes was observed, indicating that some of the material was lost. However, it was not feasible to quantify the SPION loss on these surfaces. Similarly, the amount of CpG lost during SPION-CpG synthesis is also difficult to quantify. Therefore as an approximation, the concentrations reported in subsequent experiments assumed no loss of SPIONs and no loss of CpG. At worst, when using this approximation we underestimated the immunostimulatory potential and cell uptake efficiency of SPION-CpG.

### 3.2. Mass Spectrometry

Using 3kD MWCO centrifugal spin filters (Amicon Ultra 0.5 mL, catalogue # UFC500324, EMD Millipore), crude from the RSSCpG reduction reaction was washed with an ammonium acetate – acetic acid buffer (pH = 4.5) and deionized water for desalting. The sample was introduced by nanoelectrospray into a Thermo LTQ-FT operated in negative ion mode under manual control. Ions were detected in the ICR cell at resolution 100,000 (at m/z 400).

### 3.3. NFκB activity assay

RAW-Blue™ mouse macrophage reporter cells (Invivogen) were cultured at 5000 cells per well (using a 96-well plate; 6 repeat per group). Cells were treated with 10 μL of RSSCpG, SPION-CpG, or water for 16 hours. Both RSSCpG and SPION-CpG treated wells had the same final CpG concentration (0.1 mg/mL). The level of secreted embryonic alkaline phosphatase (SEAP) was quantified by incubating 10 μL of supernatant with 190 μL QuantiBlue™ substrate (InvivoGen) for 1h and reading absorption at 620 nm using DTX 880 Multimode Detector (Beckman Coulter). QuantiBlue™ substrate was prepared by mixing one pouch of QUANTI-Blue in 100 mL of deionized water. The solution was then filtered using a 0.2 μm membrane. QuantiBlue™ substrate was warmed at 37°C prior to use.

### 3.4. Physical characterizations

Dynamic light scattering (DLS) and zeta potential (ZP) measurements were performed (ionic strength $10^{-3}$M using NaCl) on a Brookhaven 90 Plus/BI-MAS Instrument

(Brookhaven Instruments, New York). DLS measurements were obtained by performing 10 runs at 30 s per run and the ZP values by measuring 10 runs involving 20 cycles per run. For the zeta potential measurements the samples were diluted to achieve an effective concentration of 0.01 w/v% (assuming no SPION loss). Each time, prior to performing DLS and ZP measurements the sample was ultrasonicated for 1 h.

### 3.5. LIVE/DEAD staining and light microscopy

Cytotoxicity assessment was performed using the LIVE/DEAD staining assay (Invitrogen). N9 microglia cells seeded at $9.6\times10^4$ cells per well in a glass bottom cell culture dish were grown to 80% confluence. For each viability assay, the cells were washed with PBS, treated with the SPION-CpG conjugates and incubated for 12 h. After exposure to the different SPIONs, the cells were rinsed with PBS and stained with calcein-AM and ethidium homodimer (EthD-1 or EthD-2). The dyes were mixed together and appropriately diluted so that the effective working solution contains 2 μM of calcein-AM and 4 μM of ethidium homodimer which was then directly added to cells following manufacturer's protocol. After incubation with the dye, the cells were treated with fixative (either glutaraldehyde for post-movement SEM samples or paraformaldehyde) and imaged.

Light microscopy images were obtained on several instruments: Nikon Eclipse TS100 microscope equipped with Infinity2 camera (Nikon Instruments Inc., USA), Nikon Eclipse TE2000-U Inverted Fluorescence microscope (Nikon Instruments Inc., USA), Zeiss Axio Observer Z1 Inverted microscope with a Hamamatsu EMCCD C9100-13 Monochrome Camera, and a Zeiss LSM 710 confocal laser-scanning microscope with a Plan-Apochromat 20×/0.8 objective (Carl Zeiss Microimaging, Thornwood, NY). For confocal images, optical sections were collected at 1 μm spacing and shown as a maximum intensity projection using Zen 2009 software (Carl Zeiss). For the Zeiss Axio Observer, Zen 2012 blue software was used.

### 3.6. Inductively coupled plasma mass spectroscopy (ICP-MS) for uptake and exocytosis

To quantify the total uptake of the SPION-CpG by the microglia N9 cells we performed ICP-MS (4500 Series, Hewlett Packard) measurements. The cells were grown as described above and treated with various concentrations of SPION-CpG (0, 0.01, 0.1, 0.3 and 0.5 mg/mL) or Ferumoxytol (1.5 mg/mL). After 12 h of exposure, the medium was aspirated, the cells were washed once with PBS and were collected by treating with 0.2% trypsin-EDTA, followed by washing two times with PBS and table-top centrifugation (1000 rpm, 5 min), acid digested overnight using 1 mL of 67–70% BDH Aristar ® Plus Nitric Acid, and analyzed using ICP-MS upon appropriate dilution. A standard curve was made using serial dilution of a 1ppm solution of Iron standard solution (Spex CertiPrep). Iron concentration was determined by ICPMS Analysis on a HP 4500 Series using a concentric nebulizer, Scott type spray chamber, and a fixed quartz injector torch. A CX interface was used. Plasma power was 1500 Watt. Helium was used as the collosion gas (4 mL/min). Data was analyzed quantitatively in a spreadsheet program.

To evaluate exocytosis, N9 cells were plated at 6,000 cells per well in a 96 well plate (18,000 cells/$cm^2$) and allowed to adhere for 24 h. The cells were then loaded at a 0.1

mg/mL concentration of SPION-CpG for 2 h. After loading, the cells were washed twice with PBS and 150 μL fresh media was added to each well. At t = 0 h, 8 h, and 24 h, media in the well was completely removed ("supernatant" fraction) and both the amount of iron in both the supernatant and cell fractions was quantified via ICP-MS. Each group was in triplicate and two independent experiments were performed.

ICP-MS for the exocytosis experiment was performed as follows: 200 μL BDH Aristar ® Plus Nitric Acid (70%) was added to each sample tube (for the supernatant fraction) or well of a 96 well plate (cell fraction) to dissolve the iron. Each tube or well was washed once with 200 μL of 70% Nitric acid, the sample was then diluted to 3.4 mL with 3 mL of 2% nitric acid solution. Iron concentration was determined by ICPMS Analysis on Agilent 7500 Series using a concentric nebulizer, Scott type spray chamber, and a fixed quartz injector torch. A CX interface was used. Plasma power was 1500 Watt. Helium was used as the collosion gas (4 mL/min). A standard curve was made using serial dilution of a 1ppm solution of Iron standard solution (Spex CertiPrep). Data was analyzed quantitatively in a spreadsheet program.

### 3.7. Dark-field microscopy imaging

Cells were grown to 80% confluence on a glass bottom cell culture dish for 24–48 h. The cells were loaded with 0.5 mg/mL SPION-CpG for 2 h. After loading, excess media was removed, and the cells were washed extensively with PBS. The cover slips were carefully detached from the bottom of the dishes using a sharp edge forcep and allowed to dry. A drop of non-drying immersion oil (Cargille Laboratories, Cedar Glove, NJ) was put on the cover slip and the cover slip was mounted onto the glass slide and was adhered using nail polish to prevent drying. Dark-field microscopy imaging was performed using a CytoViva dark field microscope system equipped with CytoViva Hyperspectral Imaging System 1.2.

### 3.8. Electron Microscopy (SEM and TEM)

TEM imaging was performed on a FEI Tecnai 12 TEM equipped with a Gatan Ultrascan 2K CCD camera at an accelerating voltage of 120 kV. Cells treated with SPION-CpG conjugates (0.5 mg/mL) as described earlier, were collected by treating with 0.2% trypsin-EDTA, followed by washing with PBS and table top centrifugation (2000 rpm, 5 min), fixed with 2% glutaraldehyde in 0.1 M Cacodylate buffer ($Na(CH_3)2AsO_2 \bullet 3H_2O$), pH 7.2, at 4°C overnight. The following day the cells were washed three times with 0.1 M Cacodylate buffer, post-fixed with 1% $OsO_4$ in 0.1 M Cacodylate buffer for 30 min and washed three times with 0.1 M Cacodylate buffer. The samples were then dehydrated using 60%, 70%, 80%, 95% ethanol and 100% absolute ethanol (twice), propylene oxide (twice), and were left in propylene oxide/Eponate (1:1) overnight at room temperature under sealed environment. The following day the vials were left open until the propylene oxide was evaporated (~2–3 h). The samples were infiltrated with 100% Eponate and polymerized at ~64°C for 48 hours. Ultra-thin sections (~70 nm thick) were cut using a Leica Ultra cut UCT ultra-microtome equipped with a diamond knife, and the sections were picked up on 200 mesh copper EM grids. The grids were stained with 2% uranyl acetate for 10 minutes followed by Reynold's lead citrate staining for a minute prior to imaging.

SEM images of the magnetically-moved cells were obtained on an FEI Quanta 200 scanning electron microscope. Immediately after LIVE/DEAD staining, cells were fixed with 2% glutaraldehyte in 0.1M Cacodylate buffer ($Na(CH_3)_2AsO_2 \cdot 3H_2O$), pH7.2, at 4°C. The coverlip was then removed from the glassbottom dish using Coverslip Removal Fluid (MatTek) following the manufacturer's protocol. The coverslip was then washed three times with 0.1M Cacodylate buffer, pH 7.2, post-fixed with 1% $OsO_4$ in 0.1M Cacodylate buffer for 30 min and washed three times with 0.1M Cacodylate buffer. The samples were then dehydrated through 60%, 70%, 80%, 95% ethanol, 100% absolute ethanol (twice). The samples were dried in a critical-point dryer and then coated with gold and palladium (Au: Pd 60/40 ratio) in a Cressington 308R coating system.

### 3.9. Magnetic-field induced qualitative cell movement *in vitro* by bright-field microscopy

For the magnetically induced cell movement experiments, microglia N9 cells were cultured as described above. Cells were seeded at $9.3\times10^5$ cells per dish ($9.7\times10^4$ cells/cm$^2$), grown to 90% confluence and treated with various concentrations (low; 0.1 mg/mL, medium; 0.3 mg/mL and high; 0.5 mg/mL) of SPION-CpG conjugates. After 2 h of incubation, the loading medium was aspirated, the cells were washed extensively with PBS (carefully, until most of the free SPION-CpG was gone), supplemented with fresh growth medium and were placed in the incubator with magnet placed underneath the dish separately. Further to show the controlled movement of cells, three different shapes of magnets were used; square, circular, and rectangular. The movement of cells towards the magnet was assessed at various times (0 h, 2 h, 4 h and 20 h) using microscopy. In order to verify that increased iron concentration at the edge of the magnet was SPION-CpG-loaded cells and not free particles in solution, a cell-free SPION-CpG-only control was included. After movement, the cells were stained for iron using Prussian blue staining as per manufacturer's (Polyscience Inc. Warrington, PA) instructions. Briefly, equal volumes of 4% potassium ferrocyanide and 4% hydrochloric acid were mixed together to prepare the working solution. The standard staining required at least two changes of the working solution treatments for 10 minutes each. After which the cells were rinsed three times with distilled water and stained using nuclear fast red for 3 min. Finally, the cells are rinsed in running tap water for 1 minute and imaged immediately.

### 3.10. Cell box design

An imaging apparatus was required to image, incubate, and magnetically manipulate cells loaded with SPION-CpG. The apparatus, or cell box, was inserted onto a petri dish containing cell media. It was comprised of a 3D printed ABS substrate (Fig S4Q) attached to a large coverslip (48 mm × 65 mm no 1, Ted Pella, catalogue #260365). The cell box provides an enclosed environment for long term cell viability and proliferation while allowing for external manipulation of magnet fields. In order to maintain the pH of cell media, exogenous $CO_2$ was supplied through the inlet port of the custom cell box and evenly distributed to distribution channels inside the petri dish. A pressure relief port prevented the accumulation of pressure and ensured a continuous flow of atmosphere.

The cell box was printed using a 3D printer (Replicator 2, Makerbot) and is both airtight and waterproof. The cell box features a hollow center to enable light illumination during bright

field microscopy. A slotted coverslip face allows for structural support of the coverslip and coverslip adhesive. The cell box was printed with ABS filament (ABS filament, Makerbot).

### 3.11. Live cell imaging

In preparation for live cell imaging, the cell box was assembled and N9 cells plated on it. The box was first sterilized by soaking in 0.6% NaOCl and rinsed thoroughly with autoclaved deionized water in order to remove residual NaOCl (bleach). A large coverslip (48 mm × 65 mm no 1, Ted Pella, catalogue #260365) was autoclaved and attached to the cell box using a non-cytotoxic silicone based adhesive (Silbione Med Adhesive 4100 RTV, Factor II, catalogue #A-4100). The box-coverslip assembly was then left at room temperature in a sterile environment (biosafety hood) for about 2 days in order to allow the adhesive to cure. After 2 days, an autoclaved polydimethylsiloxane (PDMS) dam was placed on the coverslip in order to form a makeshift tissue culture dish. The PDMS dam was created by first synthesizing a ~0.5 cm thick rectangular slab of PDMS on a clean glass surface (Sylgard 184 Silicone elastomer kit, Dow Corning, follow manufacturer's protocol) and then cutting an ~9 $cm^2$ rectangular hole in the PDMS. When this PDMS dam is set on the box-coverslip assembly, it forms a water-tight seal with the coverslip. Once the dam is in place, N9 cells ($8.72\times10^5$ cells or $9.7\times10^4$ cells/$cm^2$) were plated on the coverslip and allowed to adhere for 8 h in the incubator. The cells were then loaded at 0.1 mg/mL SPION-CpG for 2 h, following the protocol for the previous cell movement experiment. After loading, the cells were washed with PBS, the PDMS dam was removed and the box-coverslip assembly was inverted into a 100 mm petri dish containing enough media to submerge the coverslip (10 – 20 mL).

Live cell imaging was performed on a Zeiss Axio Observer Z1 Inverted microscope with the Pecon/Zeiss Incubation System. Images were obtained using a 10×/ 0.3NA EC-Plan Neofluar objective and a Hamamatsu EMCCD C9100-13 Monochrome Camera. The microscope and camera were controlled using the Zen 2012 Blue Edition software. After connecting the cell box to the microscope, pre-magnet images were taken for reference. A ceramic magnet was then placed on top of the coverslip portion of the cell box above the region of the coverslip where cells are adhered. To prevent the magnet from moving during the experiment, the magnet was secured to the coverslip with tape. Using time-lapse imaging (1 brightfield image every 30 s), the motion of cells within one field of view near the magnet were tracked over 20 h (the same time scale used for the other movement experiment).

### 3.12. Cell tracking

Magnetized cells were imaged inside the cell box for 20 h at a frame rate of 2 frames/min in order to observe long-term motility. The centroid postion of the cell was determined using a computer vision algorithm as seen in Fig 5.[32] A 2D cross correlation was computed to determine position offsets in consecutive frames. All cells move in the same plane. The velocities of the cells were examined both in the direction of the magnet (positive vertical direction) as well as the horizontal direction, as seen in Fig 4A–B. The velocity of the cell from one frame to the next was calculated by multiplying the displacement in one frame by the frame rate.

## 4. Conclusions

SPION-CpG conjugates were non-toxic to N9 microglia cells and were efficiently internalized into endosmal compartments. This enabled magnetic control over microglia motility *in vitro*. This work establishes the possibility of using a nanoparticle to both stimulate immune cells and to control their trafficking. Future experiments will investigate the optimal coating for the SPIONs to further enhance immune cell activation.

## Supplementary Material

Refer to Web version on PubMed Central for supplementary material.

## Acknowledgements

We gratefully acknowledge ICP-MS instrumentation under the supervision of Nathan Dalleska at the Environmental Analysis Center at the California Institute of Technology. We thank Denise Keen from the Mass Spectrometry and Proteomics Core Facility at the Beckman Research Institute of the City of Hope for assistance with mass spectrometry. The authors gratefully acknowledge Marcia M. Miller, Zhuo Li and Ricardo Zerda for assistance with the TEM from the COH Electron Microscope Core Facility. The authors gratefully acknowledge Brian Armstrong and Tina Patel for assistance with fluorescent and bright field microscopy from the Light Microscopy Digital Imaging Core. The authors gratefully acknowledge Kaushik Dasgupta and Jeff Sherman for their dedicated assistance in magnetic manipulation of magnetized cells. The authors would like to also thank Brian Hong for proofreading this manuscript. Finally, the authors would like to thank ONR N00014-02-1 0958 for funding for the TEM, NSF DBI-9970143 for funding for the Ultramicrotome, R21NS081594, R01CA155769, R21CA189223, City of Hope-Caltech Biomedical Research Initiative, The Kenneth T. and Eileen L. Norris Foundation, STOP Cancer, and the ThinkCure! Foundation for research funding. Research reported in this publication included work performed in the Light Microscopy Digital Imaging and Electron Microscopy Cores supported by the National Cancer Institute of the National Institutes of Health under award number P30CA33572.

## References

1. Mellman I, Coukos G, Dranoff G. Nature. 2011; 480:480–489. [PubMed: 22193102]
2. Meng Y, Kujas M, Marie Y, Paris S, Thillet J, Delattre JY, Carpentier AF. J Neurooncol. 2008; 88:19–25. [PubMed: 18253698]
3. Hussain SF, Yang D, Suki D, Grimm E, Heimberger AB. J Transl Med. 2006; 4:15. [PubMed: 16573834]
4. Hussain SF, Yang D, Suki D, Aldape K, Grimm E, Heimberger AB. Neuro Oncol. 2006; 8:261–279. [PubMed: 16775224]
5. Bsibsi M, Ravid R, Gveric D, van Noort JM. Journal of neuropathology and experimental neurology. 2002; 61:1013–1021. [PubMed: 12430718]
6. Latz E, Schoenemeyer A, Visintin A, Fitzgerald KA, Monks BG, Knetter CF, Lien E, Nilsen NJ, Espevik T, Golenbock DT. Nature immunology. 2004; 5:190–198. [PubMed: 14716310]
7. Badie B, Berlin JM. Immunotherapy. 2013; 5:1–3. [PubMed: 23256791]
8. Dobrovolskaia MA, Aggarwal P, Hall JB, McNeil SE. Molecular pharmaceutics. 2008; 5:487–495. [PubMed: 18510338]
9. Suzuki Y, Wakita D, Chamoto K, Narita Y, Tsuji T, Takeshima T, Gyobu H, Kawarada Y, Kondo S, Akira S, Katoh H, Ikeda H, Nishimura T. Cancer Research. 2004; 64:8754–8760. [PubMed: 15574787]
10. Rattanakiat S, Nishikawa M, Takakura Y. Eur J Pharm Sci. 2012; 47:352–358. [PubMed: 22771546]
11. Demento SL, Bonafe N, Cui WG, Kaech SM, Caplan MJ, Fikrig E, Ledizet M, Fahmy TM. Journal of Immunology. 2010; 185:2989–2997.
12. Wei M, Chen N, Li J, Yin M, Liang L, He Y, Song HY, Fan CH, Huang Q. Angew Chem Int Edit. 2012; 51:1202–1206.

13. Zhao DC, Alizadeh D, Zhang LY, Liu W, Farrukh O, Manuel E, Diamond DJ, Badie B. Clinical Cancer Research. 2011; 17:771–782. [PubMed: 21088258]
14. Fan H, Zhang I, Chen X, Zhang L, Wang H, Da Fonseca A, Manuel ER, Diamond DJ, Raubitschek A, Badie B. Clin Cancer Res. 2012; 18:5628–5638. [PubMed: 22904105]
15. McBain SC, Yiu HH, Dobson J. Int J Nanomedicine. 2008; 3:169–180. [PubMed: 18686777]
16. Shapiro B. Journal of magnetism and magnetic materials. 2009; 321:1594. [PubMed: 20165553]
17. Nacev A, Kim SH, Rodriguez-Canales J, Tangrea MA, Shapiro B, Emmert-Buck MR. International Journal of Nanomedicine. 2011; 6:2907–2923. [PubMed: 22131836]
18. Chertok B, Moffat BA, David AE, Yu F, Bergemann C, Ross BD, Yang VC. Biomaterials. 2008; 29:487–496. [PubMed: 17964647]
19. Pislaru SV, Harbuzariu A, Gulati R, Witt T, Sandhu NP, Simari RD, Sandhu GS. J Am Coll Cardiol. 2006; 48:1839–1845. [PubMed: 17084259]
20. Polyak B, Fishbein I, Chorny M, Alferiev I, Williams D, Yellen B, Friedman G, Levy RJ. Proc. Natl. Acad. Sci. U. S. A. 2008; 105:698–703. [PubMed: 18182491]
21. Kyrtatos PG, Lehtolainen P, Junemann-Ramirez M, Garcia-Prieto A, Price AN, Martin JF, Gadian DG, Pankhurst QA, Lythgoe MF. JACC. Cardiovascular interventions. 2009; 2:794–802. [PubMed: 19695550]
22. Arbab AS, Jordan EK, Wilson LB, Yocum GT, Lewis BK, Frank JA. Human gene therapy. 2004; 15:351–360. [PubMed: 15053860]
23. Vanecek V, Zablotskii V, Forostyak S, Ruzicka J, Herynek V, Babic M, Jendelova P, Kubinova S, Dejneka A, Sykova E. Int J Nanomedicine. 2012; 7:3719–3730. [PubMed: 22888231]
24. Yanai A, Hafeli UO, Metcalfe AL, Soema P, Addo L, Gregory-Evans CY, Po K, Shan X, Moritz OL, Gregory-Evans K. Cell transplantation. 2012; 21:1137–1148. [PubMed: 22405427]
25. Jang ES, Shin JH, Ren G, Park MJ, Cheng K, Chen X, Wu JC, Sunwoo JB, Cheng Z. Biomaterials. 2012; 33:5584–5592. [PubMed: 22575830]
26. Laurent S, Forge D, Port M, Roch A, Robic C, Vander Elst L, Muller RN. Chemical reviews. 2008; 108:2064–2110. [PubMed: 18543879]
27. Sahoo Y, Pizem H, Fried T, Golodnitsky D, Burstein L, Sukenik CN, Markovich G. Langmuir. 2001; 17:7907–7911.
28. Haas T, Metzger J, Schmitz F, Heit A, Müller T, Latz E, Wagner H. Immunity. 2008; 28:315–323. [PubMed: 18342006]
29. Castaneda RT, Khurana A, Khan R, Daldrup-Link HE. Journal of visualized experiments : JoVE. 2011:e3482. [PubMed: 22083287]
30. Rosi NL, Giljohann DA, Thaxton CS, Lytton-Jean AK, Han MS, Mirkin CA. Science. 2006; 312:1027–1030. [PubMed: 16709779]
31. Patel PC, Giljohann DA, Daniel WL, Zheng D, Prigodich AE, Mirkin CA. Bioconjugate chemistry. 2010; 21:2250–2256. [PubMed: 21070003]
32. Hedrick TL. Bioinspiration & Biomimetics. 2008; 3:034001. [PubMed: 18591738]

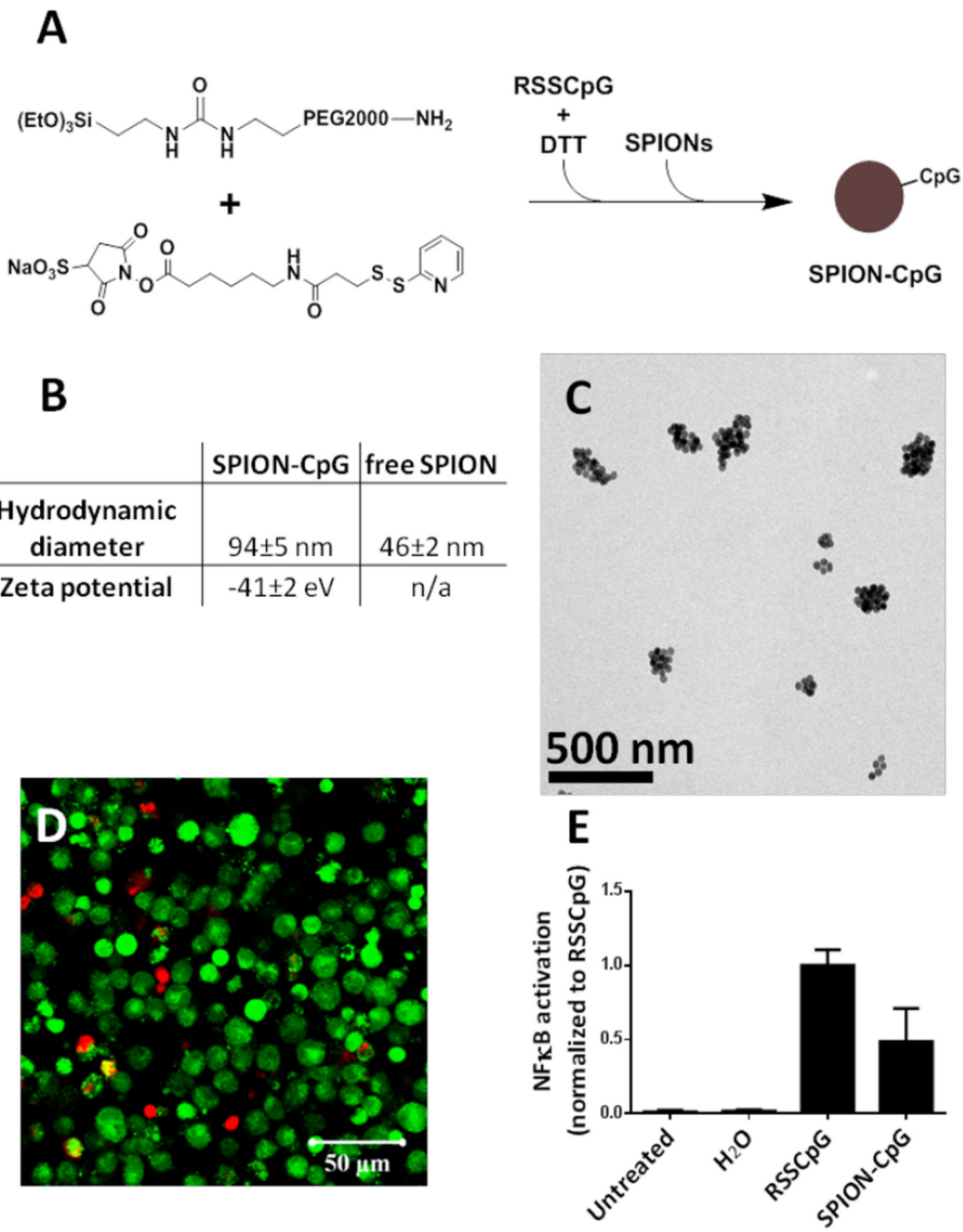


**Figure 1.**

Synthesis and characterization of the SPION-CpG conjugates. (A) Schematic illustration of the synthesis of SPION-CpG conjugates. (B) Hydrodynamic diameter and zeta potential of SPION-CpG conjugates. (C) Transmission electron microscopy image of the SPION-CpG conjugates. (D) LIVE/DEAD stain of N9 cells treated with 0.5 mg/mL for 12 h. Red = ethidium homodimer (dead), green = calcein AM (live). (E) NFκB activation of RAW-Blue™ mouse macrophage reporter cells treated with 0.1 mg/mL SPION-CpG (n=2, 6 replicates each). The average of the normalized data from two assays is shown.

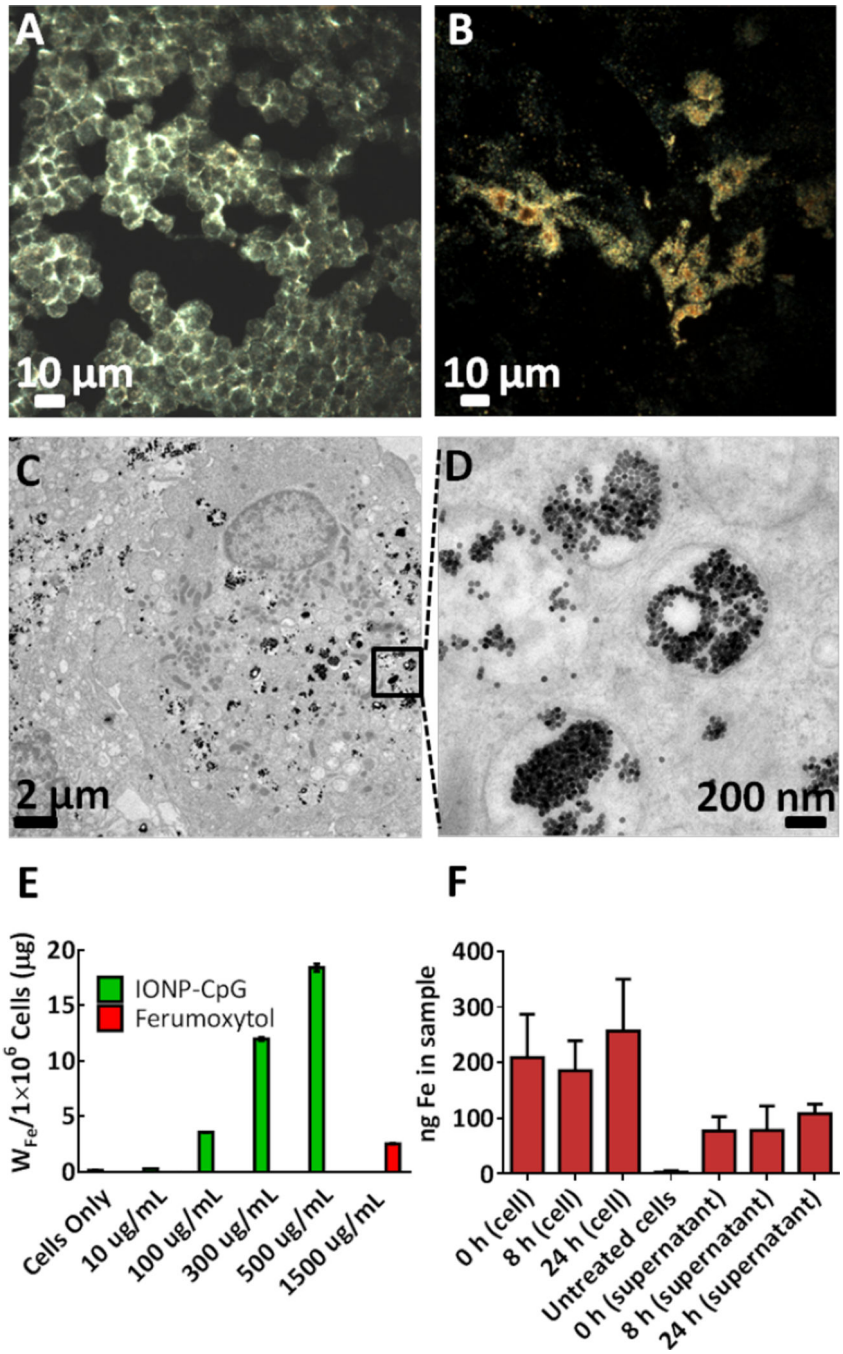


**Figure 2.**

SPION-CpG is internalized in N9 cells. Dark-field images of (A) microglia cells alone and (B) cells loaded with SPION-CpG conjugates [0.5 mg/mL]. (C–D) TEM images of loaded cells. ICP-MS analysis of (E) cells treated with increasing concentrations of SPION-CpG conjugates and Ferumoxytol. (F) Cell and supernatant fractions at various time points after loading (n=2 with treatments performed in triplicate, average of two experiments is shown). Error bars represent standard deviations of iron content in replicate wells.

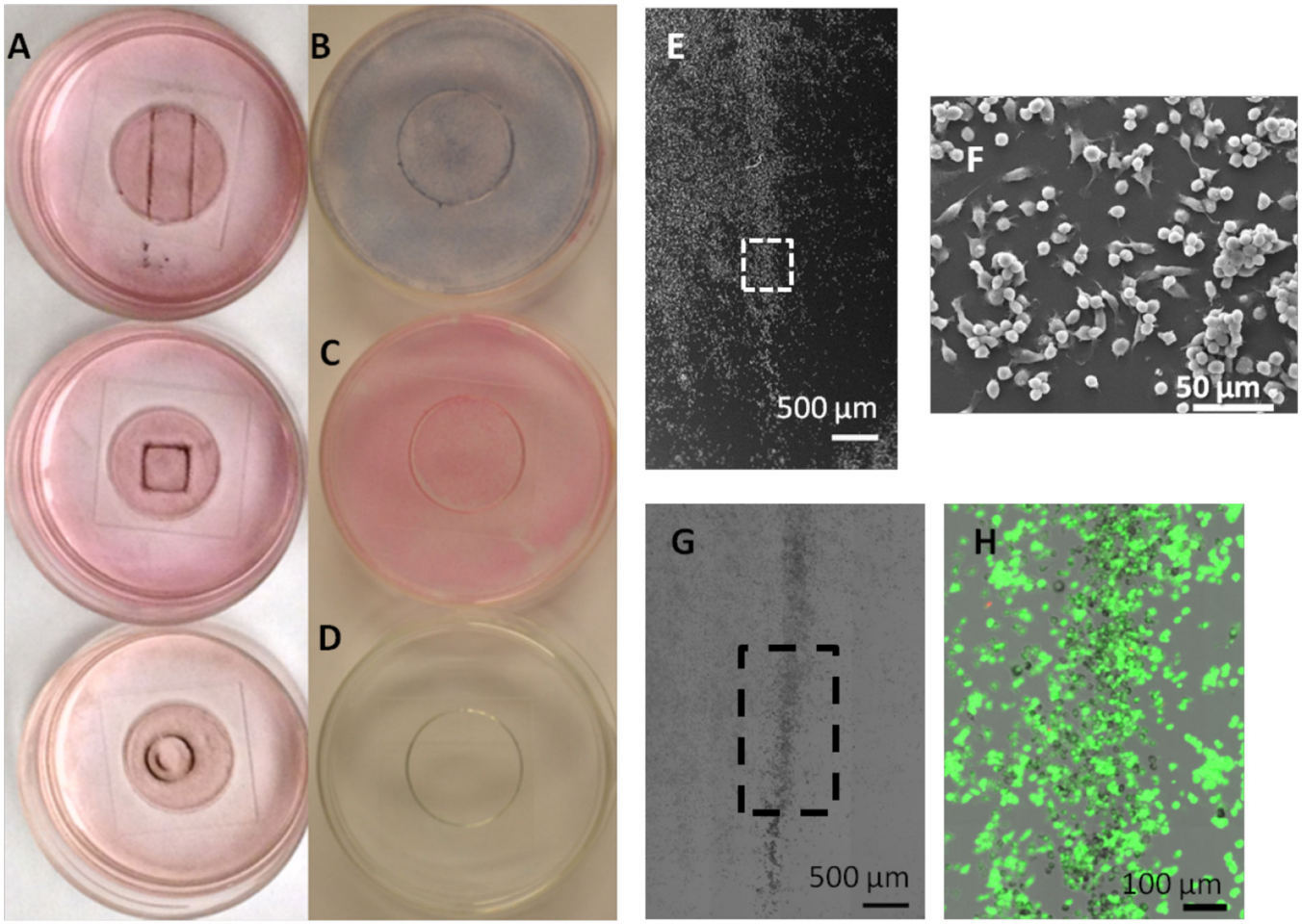


**Figure 3.**

Magnetically induced movement of the cells loaded with SPION-CpG conjugates. (A) Color images of loaded cells after exposure to magnets of different shapes for 20 h. The concentration of SPION-CpG used for loading was 0.1 mg/mL. (B–D) are the various controls used for the magnetic movement experiments; (B) loaded cells not exposed to the magnet, (C) unloaded cells exposed to the magnet, and (D) SPION-CpG only without cells. (E–F) SEM images of cells after movement. (G–H) Brightfield and fluorescent images of LIVE/DEAD-stained cells after movement.

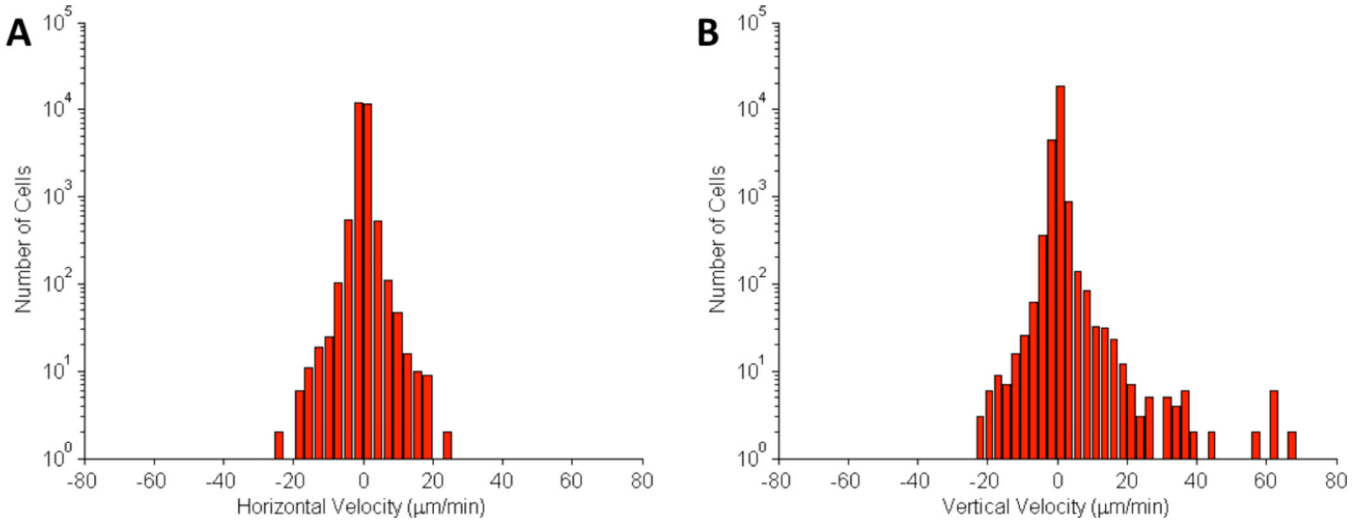


**Figure 4.**

Histograms of (A) horizontal and (B) vertical cell velocities in motility experiment. Magnetized cells were imaged over a period of 12 h under the exposure of a magnetic field. The external magnet was placed in the positive vertical position to the cells. Velocities were calculated by extracting the change in cell position from one frame to the next. The average velocity was 0.2±3.72 μm/min and the vertical direction and 0.03±1.69 μm/min in the horizontal direction.

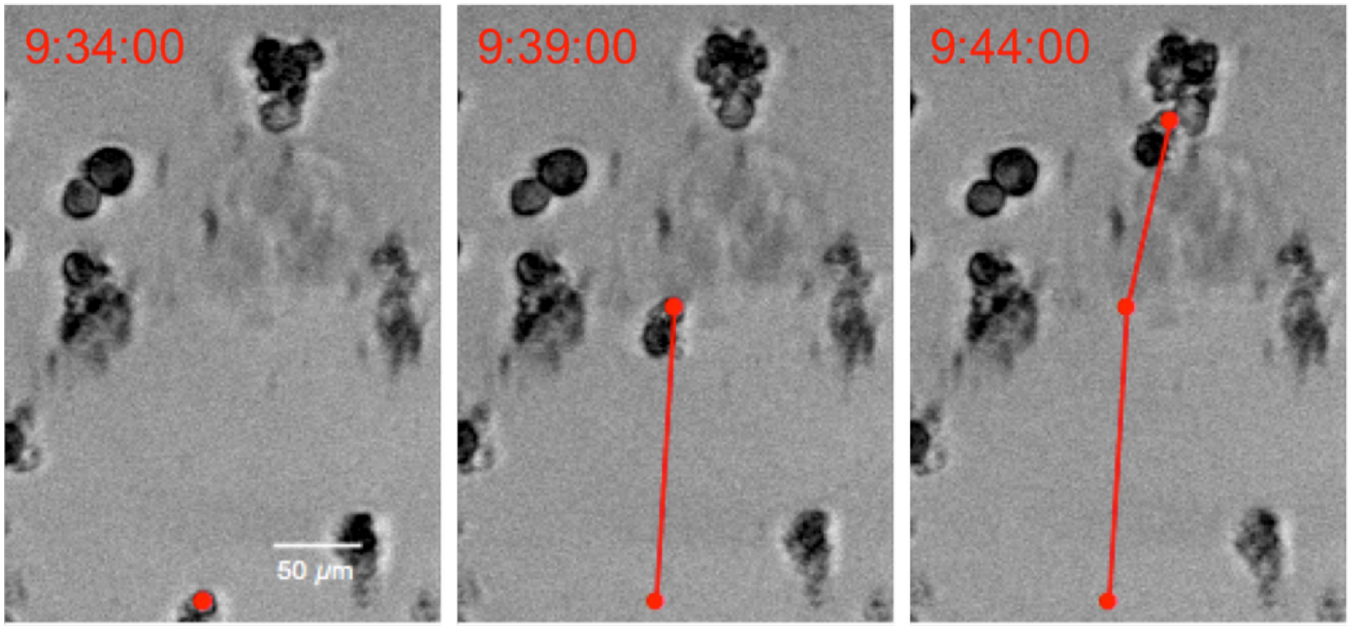


**Figure 5.**

Tracking magnetized cells under the exposure of a magnetic field. The cell position was calculated by identifying its centroid position.[32] The cell speed was calculated using the total distance traveled between consecutive frames.